Low levels of NMNAT2 compromise axon development and survival

Jonathan Gilley* [1,2], Paul Mayer [3], Gang Yu [3] and Michael P. Coleman [1,2]

[1] John van Geest Centre for Brain Repair, Department of Clinical Neurosciences, University of Cambridge, ED Adrian Building, Forvie Site, Robinson Way, Cambridge, CB2 0PY, UK.

[2] Signalling Programme, Babraham Institute, Babraham Research Campus, Cambridge, CB22 3AT, UK.

[3] Department of Neuroscience, University of Texas Southwestern Medical Center, Dallas, Texas 75390, United States.

* Correspondence to Jonathan Gilley

John van Geest Centre for Brain Repair, Department of Clinical Neurosciences, University of Cambridge, ED Adrian Building, Forvie Site, Robinson Way, Cambridge, CB2 0PY, UK.

Tel: +44-1223-331187

Fax: +44-1223 331174

E-mail: jg792@cam.ac.uk

ABSTRACT

NMNAT2 is an endogenous axon maintenance factor that preserves axon health by blocking Wallerian-like axon degeneration. Mice lacking NMNAT2 die at birth with severe axon defects in both the PNS and CNS so a complete absence of NMNAT2 in humans is likely to be similarly harmful, but probably rare. However, there is evidence of widespread natural variation in human *NMNAT2* mRNA expression so it is important to establish whether reduced levels of NMNAT2 have consequences that impact health. Whilst mice that express reduced levels of NMNAT2, either those heterozygous for a silenced *Nmnat2* allele, or compound heterozygous for one silenced and one partially silenced *Nmnat2* allele, remain overtly normal into old age, we now report that *Nmnat2* compound heterozygote mice present with early and age-dependent peripheral nerve axon defects. Compound heterozygote mice already have reduced numbers of myelinated sensory axons at 1.5 months and lose more axons, likely motor axons, between 18 and 24 months and, crucially, these changes correlate with early temperature insensitivity and a later-onset decline in motor performance. Slower neurite outgrowth and increased sensitivity to axonal stress are also evident in primary cultures of *Nmnat2* compound heterozygote superior cervical ganglion neurons. These data reveal that reducing NMNAT2 levels below a particular threshold compromises the development of peripheral axons and increases their vulnerability to stresses. We discuss the implications for human neurological phenotypes where axons are longer and have to be maintained over a much longer lifespan.

INTRODUCTION

Axon degeneration is an early pathology in several neurodegenerative disorders and in many cases the underlying mechanism is related to injury-induced (Wallerian) degeneration (1). Wallerian degeneration proceeds via a conserved pathway in which nicotinamide mononucleotide adenylyltransferase (NMNAT) activity, a central activity during NAD biosynthesis, acts as a key regulator (1). Of the three NMNAT isoforms in mammals, NMNAT2 appears to have the most influence over axon survival under physiological conditions as only depletion of this isoform causes a primary axonal phenotype either *in vitro* or *in vivo* (2-6).

Homozygous *Nmnat2* gene trap mice lacking detectable NMNAT2 have a severe axon outgrowth defect resulting in widespread axon truncation in both the PNS and CNS that is incompatible with post-natal survival (3, 5). Importantly, the underlying defect involves a Wallerian-like mechanism as three unrelated genetic manipulations that strongly delay Wallerian degeneration - the slow Wallerian degeneration (Wld^S) mutation, knockout of the *Sarm1* gene encoding the pro-degenerative sterile alpha and TIR motif-containing protein 1 (SARM1), and a bacterial nicotinamide mononucleotide (NMN) deamidase transgene - all improve axon outgrowth and rescue lethality (3, 7, 8). Remarkably, mice rescued by *Sarm1* deletion remain overtly normal up to 2 years (9).

Single nucleotide polymorphisms (SNPs) within the *NMNAT2* gene show genome-wide significant association with human cognition (10) and a positive correlation between cognition and *NMNAT2* mRNA levels has been identified (11). Reduced *NMNAT2* mRNA levels are also seen in Parkinson's, Alzheimer's and Huntington's disease patients (11, 12) and *Nmnat2* mRNA levels are reduced prior to the onset of pathological changes in a mouse model of tauopathy (13). These observations suggest that constitutively low or declining expression of this key regulator of axon health might contribute to clinical and sub-clinical phenotypes. Crucially,

NMNAT2 mRNA levels appear to vary widely between individuals in the human population (11), so a better understanding of how reduced (but not absent) *NMNAT2* expression influences axon survival, either constitutively or in response to neurodegenerative stresses, is needed.

Mice heterozygous for a silenced *Nmnat2* allele are viable (3, 5) and, other than reduced expression of synaptic proteins in the hippocampus (11) and cortical neurons that are modestly more sensitive to the chemotherapeutic agent vincristine in culture (14), they otherwise appear superficially normal up to at least 12 months of age (3, 14). In fact, PNS and CNS axon outgrowth and several baseline or induced behaviors, including their response to vincristine *in vivo*, are unaltered (3, 5, 14). Thus, current observations suggest a halving of NMNAT2 expression has relatively limited effects on neural development and maintenance in mice. However, by studying compound heterozygous mice with one silenced and one partially silenced *Nmnat2* allele (3), we now show that sub-heterozygous *Nmnat2* expression results in the absence and/or loss of specific peripheral nerve axon populations and that this correlates with changes to baseline responses in specific behavioral tests. Outgrowth of neurites and their resistance to vincristine toxicity are also compromised in primary cultures of superior cervical ganglion (SCG) neurons. The possibility that the development of much longer human axons and their ability to cope with neurodegenerative stresses, including normal ageing over a much greater lifespan, could be similarly affected by comparably low NMNAT2 expression will have important implications in relation to disease susceptibility and clinical outcomes.

RESULTS

Mice with low level *Nmnat2* expression are viable and overtly normal

We previously crossed mice heterozygous for two distinct *Nmnat2* gene trap alleles with different degrees of gene silencing, *Nmnat2*^{gtE} and *Nmnat2*^{gtBay}, to generate mice with graded levels of *Nmnat2* mRNA and NMNAT2 protein expression (3). Whilst a gene trap cassette is located in the large first intron of the *Nmnat2* gene in each case, the *Nmnat2*^{gtE} allele appears to be completely silenced (3) whereas the *Nmnat2*^{gtBay} allele is only partially silenced and retains ~50% of normal expression (15). Mice of all four genotypes produced from these crosses, including *Nmnat2*$^{gtBay/gtE}$ compound heterozygotes with the lowest, sub-heterozygous levels of expression, were reported to be viable and overtly normal up to 12 months of age (3).

We now confirm that genotype ratios for offspring of these crosses are not significantly different from that expected (Fig. 1A), that there is no significant difference in body weight between genotypes at either 6 or 24 months (Fig. 1B), and that no genotype can be distinguished from littermates based on appearance or home cage behavior. Whereas *Nmnat2* mRNA levels in the brains of newborn *Nmnat2*$^{+/gtE}$ single heterozygote pups or late-stage embryos are consistently almost exactly 50% of that in wild-types (3, 8), we found levels to be around 60% in 6 month old mice (Fig. 1C). This could reflect a change in splicing that modestly alters the efficiency of *Nmnat2*^{gtE} gene trap silencing and/or compensatory up-regulation or stabilization of *Nmnat2* mRNA expressed from the wild-type allele. Nevertheless, the amount of *Nmnat2* mRNA in the brains of adult *Nmnat2*$^{gtBay/gtE}$ compound heterozygote mice, at around 30% of wild-type levels, is still well below a true heterozygous level of 50% (Fig. 1C). These findings confirm that *Nmnat2* expression can be reduced to sub-heterozygous levels in mice without compromising long-term viability and without any effect on overt morphology or behavior.

Nmnat2 compound heterozygote mice have an early deficiency of myelinated sensory axons with later-onset motor axon changes

Given that NMNAT2 is critically required for axon development and survival (3, 5), we assessed whether there was any loss of peripheral axons in either *Nmnat2*$^{+/gtE}$ single heterozygote or *Nmnat2*$^{gtBay/gtE}$ compound heterozygote mice compared to wild-types. We initially performed counts of myelinated axons in the tibial nerve, at mid-calf level, of 6 and 24 month old mice. The number of myelinated axons in *Nmnat2*$^{+/gtE}$ single heterozygotes was comparable to wild-types at both ages with no evidence of substantial axon loss between 6 and 24 months in either (Fig. 2A). In contrast, we found that *Nmnat2*$^{gtBay/gtE}$ compound heterozygote mice already had around 25% fewer myelinated tibial nerve axons at 6 months and showed a further reduction at 24 months (Fig. 2A). An extended analysis, specifically in nerves from *Nmnat2*$^{gtBay/gtE}$ and wild-type mice at 1.5 and 18 months, revealed that a reduction in axon numbers in *Nmnat2*$^{gtBay/gtE}$ nerves was already evident at 1.5 months and remained stable up to 18 months, with the additional axon loss occurring after this age (Fig. 2B). The relative deficiency of axons in *Nmnat2*$^{gtBay/gtE}$ nerves at each age was matched by a proportional reduction in nerve cross-sectional area such that axon density remained similar to wild-types at each age (Fig. 2C and 2D). These observations are consistent with a constitutive deficiency, or a very early loss, of myelinated tibial nerve axons in *Nmnat2*$^{gtBay/gtE}$ mice followed by some additional, slowly-progressing loss in old age.

We next assessed numbers of myelinated axons in dorsal and ventral roots close to the L3 dorsal root ganglion (DRG) of 6 and 24 month wild-type and *Nmnat2*$^{gtBay/gtE}$ mice. L3 roots contribute a significant proportion of axons to the tibial nerve in mice (16) and were thus used to determine whether sensory or motor axons are missing from *Nmnat2*$^{gtBay/gtE}$ tibial nerves at either age. We found that there were around 30% fewer myelinated axons in the L3 dorsal roots of *Nmnat2*$^{gtBay/gtE}$ compound heterozygotes compared to wild-types at 6 months, with no further

reduction at 24 months (Fig. 3A). Measurement of axon diameters revealed a specific reduction in small diameter (1-3 μm) myelinated axons, presumably Aδ fibers, in the *Nmnat2*$^{gtBay/gtE}$ roots (Fig. 3B). Crucially, the remaining axons appeared morphologically normal, even at 24 months (Fig. 3C). In contrast, myelinated motor axon numbers and morphology in *Nmnat2*$^{gtBay/gtE}$ L3 ventral roots were comparable to wild-types at 6 months, but by 24 months we observed a substantial increase in axons with unusually thin myelin sheaths relative to axon diameter, resembling regenerating fibers, counteracting a proportionately smaller reduction in the numbers of axons with normal morphology (Fig. 3D, 3E and 3F). The number of axons with abnormal myelin (invaginations, evaginations or wide incisures) was not altered (Fig. 3F). Intriguingly, this resulted in an overall increase in the total number of myelinated axons in the *Nmnat2*$^{gtBay/gtE}$ ventral roots (Fig. 3D). A plausible explanation for these observations is that slowly progressing motor axon loss in old *Nmnat2*$^{gtBay/gtE}$ mice triggers a robust regeneration response with some axonal sprouting.

Together, these results suggest that an early deficiency of myelinated axons in *Nmnat2*$^{gtBay/gtE}$ compound heterozygote tibial nerve is due to a constitutive deficiency, or very early loss, of small caliber myelinated sensory axons, whereas a later, age-dependent loss of myelinated axons in tibial nerve from 18 months onwards probably reflects motor axon loss. Putative regenerating axons that are evident in L3 ventral roots were not seen in tibial nerve at mid-calf level suggesting they do not extend that far.

Early deficiency in thermal discrimination and age-dependent decline in Rotarod performance in *Nmnat2*$^{gtBay/gtE}$ compound heterozygote mice

We next performed a series of behavioral tests to assess whether any baseline sensory and motor functions, not apparent from normal cage activity, are altered in *Nmnat2*$^{gtBay/gtE}$ compound heterozygote mice as a result of the constitutive and age-dependent reductions in

axon numbers. Three main tests were employed: the two-plate thermal place preference test, which assesses thermal perception; the plantar aesthesiometer, which assesses mechanical sensitivity in the hindpaw; and the accelerating Rotarod, which assesses motor function and proprioception. All three tests provide objective measures of behavior.

Interestingly, using the same groups of 6-9 month male mice, we saw no differences between genotypes in the plantar aesthesiometer test, but did find altered sensitivity to non-harmful hot and cold temperatures in the two-plate thermal place preference test. Wild-type, *Nmnat2*$^{+/gtE}$ single heterozygote and *Nmnat2*$^{gtBay/gtE}$ compound heterozygote mice all responded similarly to increasing probe force in the plantar aesthesiometer test, either in terms of the average force at which hindpaw withdrawal occurred or the average latency to withdrawal (Fig. 4A). In contrast, *Nmnat2*$^{gtBay/gtE}$ compound heterozygotes showed substantially reduced avoidance of cool (15°C) and warm (40°C and 45°C) test plates compared to wild-types in the two-plate thermal place preference test (control plate set at a preferred 30°C) (Fig. 4B). At a more noxious cold temperature (5°C) there was a similar trend that was not significant in these experiments (Fig. 4B). *Nmnat2*$^{+/gtE}$ single heterozygote mice, on the other hand, did not show any statistically-significant differences compared to wild-types for any test temperature, although avoidance of the 15°C and 40°C test plates was intermediate between wild-type and *Nmnat2*$^{gtBay/gtE}$ mice with a large degree of variability within the group (Fig. 4B).

Differences between genotypes were also seen on the accelerating Rotarod. Groups of female mice were longitudinally tested every three months between 6 and 24 months of age. No age-related change in latency to fall was seen for any genotype up to 18 months (Fig. 4C) and differences between genotypes did not reach statistical significance up to this age (Fig. 4D). However, the performance of *Nmnat2*$^{gtBay/gtE}$ compound heterozygote mice declined from 18 months onwards (Fig. 4C), such that by 24 months there was a statistically-significant

reduction in their latency to fall compared to wild-types (Fig. 4D). Notably, this decline in Rotarod performance was not accompanied by a clasping phenotype when *Nmnat2*$^{gtBay/gtE}$ mice were suspended by their tails suggesting normal proprioception (data not shown). No age-dependent decline in performance was seen for *Nmnat2*$^{+/gtE}$ single heterozygote mice (Fig. 4C), although latency to fall was consistently slightly reduced compared to wild-types for this particular group (Fig. 4D). Average body weight for each genotype was comparable at all ages ruling it out as a confounding factor (Fig. 4E).

Notably, an early defect in thermal perception and later, progressive deterioration of motor performance from 18 months onwards in *Nmnat2*$^{gtBay/gtE}$ mice is broadly consistent with the constitutive or early loss of peripheral sensory axons and the later-onset motor axon changes seen in *Nmnat2*$^{gtBay/gtE}$ L3 dorsal and ventral roots and tibial nerve.

Sub-heterozygous levels of NMNAT2 alter outgrowth and vulnerability of SCG neurites

An absence of NMNAT2 severely restricts neurite outgrowth in primary neuronal cultures, whereas a halving of NMNAT2 expression has no obvious effect (3). We therefore investigated whether sub-heterozygous levels of *Nmnat2* expression might compromise neurite outgrowth in DRG or superior cervical ganglion (SCG) primary explant cultures. Surprisingly, no differences in neurite outgrowth were seen between genotypes in explant cultures of embryonic day 13.5-14.5 DRGs (data not shown), but we did find that the rate of neurite outgrowth in postnatal day 0-2 *Nmnat2*$^{gtBay/gtE}$ compound heterozygote SCG explant cultures was reduced relative to both wild-types and *Nmnat2*$^{+/gtE}$ single heterozygotes (Fig. 5A and 5B). Outgrowth slowed from 2-3 days *in vitro* (DIV2-3) such that by DIV7 *Nmnat2*$^{gtBay/gtE}$ SCG neurites were on average around 20 percent shorter (Fig. 5B). Thus, sub-heterozygous levels of *Nmnat2* expression can compromise neurite outgrowth in some neuron types.

The late loss of motor axons in *Nmnat2*$^{gtBay/gtE}$ compound heterozygote nerves also suggests that axons with reduced levels of NMNAT2 are more sensitive to natural, age-associated stresses. We therefore tested whether we could artificially replicate this increased sensitivity by assessing the effects of vincristine specifically on neurite health in primary SCG explant cultures. Vincristine triggers Wallerian-like degeneration of neurites of peripheral neurons in primary culture (17-19) likely by inhibiting fast axonal transport (20). We identified 1 nM to be the lowest single dose of vincristine that did not reproducibly trigger neurite degeneration for any genotype (data not shown), but found that daily treatment with 1 nM vincristine produced a very slowly progressing degeneration of distal neurites, primarily characterized by blebbing, that was accelerated specifically in the *Nmnat2*$^{gtBay/gtE}$ compound heterozygote cultures (Fig. 5C and 5D). Thus, *Nmnat2*$^{gtBay/gtE}$ SCG neurites appear more sensitive to vincristine-induced degeneration than either wild-type or *Nmnat2*$^{+/gtE}$ neurites. Importantly, this effect on neurites is probably distinct from the loss of neuronal viability associated with high dose vincristine seen in cortical cultures where single heterozygote *Nmnat2*$^{+/gtE}$ neurons are slightly more sensitive than wild-types (14).

Finally, given the prediction that rapid NMNAT2 loss in transected axons acts as a critical, early initiating trigger for degeneration (4), we tested whether different steady-state levels of NMNAT2 influence the timing of Wallerian degeneration in SCG explant cultures. Intriguingly, the latent phase between injury and the onset of frank degeneration was comparable between cut wild-type and *Nmnat2*$^{+/gtE}$ neurites but appeared to be accelerated in cut *Nmnat2*$^{gtBay/gtE}$ neurites (Fig. 5E). Whilst *Nmnat2*$^{gtBay/gtE}$ neurites did appear slightly less healthy at the time of transection, possibly reflecting that the distal ends of a few cannot be supported effectively with that level of NMNAT2 expression, the relative rate of degeneration was still found to be accelerated by around one hour (Fig. 5F). Reducing NMNAT2 levels can

thus accelerate Wallerian degeneration but only when starting levels are below a certain threshold.

DISCUSSION

The findings presented here indicate that constitutively low NMNAT2 levels in mice are not phenotypically neutral, at least below a threshold level, but can significantly affect the development, survival and vulnerability of peripheral axons to the extent that axon loss occurs and specific behaviors are impaired. Whilst these changes are only evident in mice when steady-state levels are substantially below a theoretical heterozygous level of 50% of normal expression, a more modest reduction in NMNAT2 functionality in humans could have a similar outcome given their longer axons, extended lifespan and greater exposure to environmental stresses. Indeed, the human *NMNAT2* gene shows an unusually low population frequency of splicing and frameshift mutations predicted to result in heterozygous loss-of-function, at least within the Exome Aggregation Consortium (ExAC; http://exac.broadinstitute.org) (21) which excludes individuals with pediatric disease. The probability of loss-of-function intolerance (pLI) of 0.94 places *NMNAT2* within the top decile of human genes for intolerance of haploinsufficiency (22) implying that heterozygosity in humans has a significantly worse outcome than in mice. However, this will need to be confirmed in future studies. Nevertheless, the reported 50-fold or more variation in *NMNAT2* mRNA levels in human post-mortem brains (11), presumably resulting from natural variation in gene regulation, raises the real possibility that NMNAT2 functionality in a significant number of individuals will be reduced to a level at which susceptibility of certain axon populations to age-related, toxin-induced or disease-dependent stresses is increased thereby predisposing them to peripheral axonopathy. The fact that *Nmnat2*$^{gtBay/gtE}$ neurites are more susceptible to vincristine toxicity *in vitro* suggests that chemotherapy-induced peripheral neuropathy, which has already been shown to involve a Wallerian-like process *in vivo* (23), is one specific human disorder where variation in NMNAT2 levels could influence outcome.

An early deficiency of some small caliber myelinated sensory axons in the L3 dorsal roots of *Nmnat2*$^{gtBay/gtE}$ compound heterozygote mice suggests that a subset of Aδ fiber DRG neurons are particularly sensitive to low NMNAT2 levels. Proximity of the axon loss to the DRG suggests that their neurons are probably also absent and a pattern of compromised axon outgrowth precipitating loss of viability due to a lack of trophic support during embryonic or early postnatal development is likely. The lack of any clear neurite outgrowth defect in *Nmnat2*$^{gtBay/gtE}$ DRG explant cultures appears to contradict this model, but compromised outgrowth from the subset of affected Aδ fiber neurons could easily be masked by normal outgrowth from the other, more abundant DRG neurons. Alternatively, affected Aδ fiber DRG neurons may already be absent by E13.5 or their neurites may not extend far enough in culture for a defect of longer *in vivo* axons to be seen. However, the retarded neurite outgrowth seen in SCG neuron cultures indicates that sub-heterozygous NMNAT2 levels can be limiting in some contexts. In contrast, low NMNAT2 levels seem to only affect motor axon survival late in life, and likely only from 18 months onwards (an absence of sensory axons is seemingly able to fully account for the deficiency of myelinated tibial nerve axons up to this age). In this respect, the previously observed reduction in anterograde trafficking of NMNAT2 in sciatic nerve axons between 18 and 24 months (24) could cause NMNAT2 levels to decline even further in *Nmnat2*$^{gtBay/gtE}$ distal axons such that they consequently drop below the critical threshold for motor axon survival which precipitates dying-back degeneration. The presence of an apparent regenerative response suggests that the motor neurons themselves remain viable, at least in the short-term.

Our findings thus reveal significant heterogeneity not only between, but also within, different peripheral neuron populations with respect to the sensitivity of their axons to low NMNAT2 levels. Natural variation in expression of NMNAT2 between different neuron types or sub-types and/or an ability to maintain its supply into axons is one possible explanation.

Alternatively, variation in axonal levels of other key molecules in the Wallerian degeneration pathway could determine survival, even when NMNAT2 levels are equivalent. However, currently-available NMNAT2 antibodies lack the sensitivity and/or specificity for reliable, quantitative immunostaining and/or immunoblotting of nerve tissue meaning this cannot yet be determined.

Silencing of a single *Nmnat2*^{gtE} allele in primary SCG neuron cultures is sufficient to cause neurite degeneration (3), so the lack of peripheral axon loss in *Nmnat2*$^{+/gtE}$ single heterozygote mice, even in old age, further highlights the apparent discrepancy between the effects of constitutive or acute reduction of NMNAT2 levels. We have previously argued that compensatory changes during early development may partially reduce the dependence on NMNAT2 thereby lowering the NMNAT level required for maintaining axon health (3). Such changes have yet to be identified but do not appear to involve altered expression of other key enzymes in the NAD-biosynthetic pathway (3). Other than altering the NMNAT2-dependent survival threshold for axons, invoking compensatory changes as a response to reduced NMNAT2 does not alter our interpretation of the main findings reported here, but it could provide an explanation for why Wallerian degeneration is only accelerated in *Nmnat2*$^{gtBay/gtE}$ compound heterozygote neurites and not in *Nmnat2*$^{+/gtE}$ single heterozygote neurites. Based on a model of Wallerian degeneration in which rapid NMNAT2 loss in transected axons, as a result of natural turnover, is an early trigger for degeneration (4), the latent phase before frank degeneration would be predicted to be accelerated by one half-life of NMNAT2 turnover, around 40 minutes (25), in cut *Nmnat2*^{gtE} neurites and by two half-lives in cut *Nmnat2*$^{gtBay/gtE}$ neurites. However, compensatory changes could, up to a point, make the duration of the latent phase dependent on other factors such that it is only shortened when NMNAT2 levels drop below a lower threshold to become limiting.

Whilst it is easy to correlate motor axon changes to the declining motor performance seen in old *Nmnat2*$^{gtBay/gtE}$ mice, the link between the early deficiency of a substantial proportion of Aδ fibers and sensory behaviors in the mice is more complicated given the varying contributions of different sensory fiber types both to peripheral thermosensation and mechanosensation (26, 27). Some Aδ fibers are involved in thermosensation, so loss of this type likely contributes to the reduced temperature discrimination seen in *Nmnat2*$^{gtBay/gtE}$ mice, although the majority are also involved in mechanosensation (28, 29). The unaltered response of *Nmnat2*$^{gtBay/gtE}$ mice to non-painful pressure is therefore intriguing. Our findings should thus act as a useful starting point for future, more focused studies of sensory perception in these mice, including an assessment of unmyelinated C fibers.

Whilst this study was focused solely on peripheral axons, it will be important to determine whether survival of specific populations of CNS axons is also compromised when NMNAT2 levels are low. Peripheral axon defects caused by low NMNAT2 appear largely restricted to *Nmnat2*$^{gtBay/gtE}$ compound heterozygote mice with sub-heterozygous expression, at least within the confines of the parameters assessed here, but there is already a suggestion that some CNS neuron / axon populations might be affected even in *Nmnat2*$^{+/gtE}$ single heterozygotes (11, 14). It will thus be interesting to establish whether these specific populations are more severely affected in *Nmnat2*$^{gtBay/gtE}$ mice and/or whether CNS axon defects are generally more widespread. Furthermore, it will be important to determine whether any central pathways also contribute to the sensory or motor defects identified in *Nmnat2*$^{gtBay/gtE}$ mice in this study.

In summary, we have shown that sub-heterozygous NMNAT2 levels can influence peripheral axon development and survival in mice in both an age-dependent and neuron type-dependent manner and that this correlates with behavioral changes. Crucially, as discussed above, reduced NMNAT2 function could have a greater impact in longer and more long-lived human axons. The wide range of *NMNAT2* mRNA expression reported in humans, together

with the possibility that some natural coding variants might also impair NMNAT2 activity, already suggests this is likely to be clinically relevant, especially during ageing when NMNAT2 axonal transport declines (24), or in pathological situations where its transport or synthesis is further perturbed. Intrinsic variation in NMNAT2 expression and/or function in humans could thus underlie differential responses to chemotherapy, diabetes or any other stresses that promote Wallerian-like axon degeneration.

MATERIALS AND METHODS

Mouse breeding, genotyping and usage

Animal work was approved by the Babraham Institute Animal Welfare, Experimentation and Ethics Committee and was performed in accordance with the Animals (Scientific Procedures) Act, 1986, under Project License PPL 70/7620. Generation of mice bearing the *Nmnat2*^{gtE} and *Nmnat2*^{gtBay} gene trap alleles and crosses to generate *Nmnat2*$^{gtBay/gtE}$ compound heterozygotes have been described (3, 15).

We performed separate duplex PCR to assess transmission of the two gene trap alleles using the following primers: primers 5'-gctggcctaggtggtgatttgc-3' (forward for wild-type), 5'-agtcatagacactagacaatcgg-3' (forward for gene trap), and 5'-actgggatgcacgagaccctgc-3' (reverse for both) to amplify a 552-bp product from the *Nmnat2*^{gtE} gene trap allele and a 491-bp product from the corresponding wild-type locus with primer annealing at 60°C and extension at 68°C (3); and primers 5'-, 5'-aggaagcagggagaggcag-3' (reverse for wild-type) and 5'-tgcaaggcgattaagttgggtaacg-3' (reverse for gene trap), and gagccacagactagtgactggttg-3' (forward for both) to amplify a 206-bp product from the *Nmnat2*^{gtBay} gene trap allele and a 310-bp product from the corresponding wild-type locus with primer annealing and extension both at 65°C.

All mice used in this work were from the same breeding colony and littermates were used wherever possible. Female mice were preferentially used in long-term ageing studies to avoid having to house lone males for long periods, although axon counts at 24 months were confirmed in at least one male of each genotype.

Reverse transcriptase-PCR (RT-PCR)

Semi-quantitative endpoint RT-PCR was used to assess *Nmnat2* mRNA expression in whole mouse brain using the same primers and conditions as described previously (3).

Analysis of myelinated axons in tibial nerves and L3 roots

The lower leg and vertebral columns of mice were fixed in 4% paraformaldehyde in 0.1M PBS (p.H. 7.4). For tibial nerves, blocks of calf muscles from mid-way between knee and ankle of the lower leg were cryosectioned at 20 µm such that the sections contained transverse sections of the nerve. For L3 dorsal and ventral roots, the L3 DRG was dissected out of the vertebral column along with its associated roots and mixed nerve and cryosectioned at 20 µm to produce transverse sections of the roots less than 1 mm from the DRG itself. Sections were then stained with FluoroMyelin™ Red (Life Technologies) according to the manufacturer's instructions. The tibial nerve was easily identified based on its size and position relative to different muscle groups in the calf.

Images of tibial nerves and L3 roots were captured on an Olympus FV1000 point scanning confocal microscope imaging system (40x objective). Axon counts (inferred from numbers of myelin sheaths), nerve cross-sectional area and axon diameters were determined using tools in ImageJ/Fiji software . Axon counts were performed blind. Axon diameter was measured as the maximum internal diameter of the myelin sheath for all axons in adjacent 500 μm^2 grid boxes running diagonally across the nerve cross-section to randomly sample at least 145 axons from each nerve analyzed. Axon diameter and nerve cross-sectional area were only measured for nerves where a true transverse section was obtained.

Mouse behavior tests

Dynamic Plantar Aesthesiometer. Touch sensitivity was assessed using a Dynamic Plantar Aesthesiometer (Ugo Basile, Varese, Italy). The apparatus automatically recorded the latency and force at the time of the paw withdrawal reflex in response to increasing pressure of a steel probe (0.5 mm diameter) applied to the plantar surface of either hindpaw of the mice. Mice were familiarized to the apparatus for 1 h prior to testing. Probe force increased up to 5 g over an initial 10 s period and this was maintained for a further 20 s for a maximum trial time of 30 s. The average latency and force at paw withdrawal was calculated from five valid trials for each mouse (trials where paw withdrawal occurred due to spontaneous movements were discounted).

Two-place Temperature Preference. Thermal preference was tested using a two-place thermal place preference apparatus (Bioseb, Vitrolles, France). Mice were placed in a run consisting of adjacent plates that can be set at different temperatures. In tests mice were offered a choice between a comfortable temperature of 30°C on one plate and a variable test temperature on the other. Mice were able to freely move between the two plates in the run and the time spent on each plate during a 5 min period was recorded automatically. Each mouse was tested for avoidance of warm and cold temperatures in two separate sessions on consecutive days. Duplicate trials were run sequentially for each test temperature, switching the test and reference plates, to control for positional preferences (independent of temperature) or memory of previous trials. Mice stayed in the runs between trials as plates cooled/warmed at their maximum rate. The percentage time spent at each test temperature was averaged from the two plate orientations for that temperature. For the 30°C/30°C preference each plate was considered the test plate for one half of the 5 min trial period to control for positional preferences. There was no statistically-significant difference between genotypes in overall distance travelled or

number of transitions between plates in the 30°C/30°C preference trial ruling out locomotor activity as a confounding factor in the changes in avoidance seen at other temperatures.

Accelerating Rotarod. Locomotor performance and balance were tested on an accelerating Rotarod (Ugo Basile, Model 7650, Varese, Italy). Mice were familiarized with the apparatus (two 5 min runs at 10 rpm) one day before the first test age. Mice were tested at 3 month intervals from 6 to 24 months of age. The majority of the mice were tested at all ages, although small numbers of mice were added at later ages to supplement natural losses. At each age mice performed three 5 min trials, where rotation increased from 3 to 30 rpm, separated by 30 min rests. The latency to fall (max 300 s) was recorded only for involuntary falls. Mice dismounting voluntarily were put back on the apparatus once but were excluded from the analysis if this was repeated. Best trial performance was used for statistical analyses.

Primary neuronal explant cultures

Superior cervical ganglia (SCG) were dissected from postnatal day 0-2 mouse pups and dorsal root ganglia (DRG) were dissected from E13.5-E14.5 mouse embryos and cultured essentially as described previously (3). Images of neurites were captured using a Soft Imaging Systems (SIS) F-View camera linked on an Olympus IX81 inverted microscope. For each of the analyses described below the effects of manipulations were recorded from both SCGs from each mouse pup and multiple DRGs from each mouse embryo and these were averaged to give an animal average. Animal averages were then used to generate genotype means.

Radial neurite outgrowth from SCG and DRG ganglia was assessed from low magnification (4x objective) phase contrast images on each specified day after plating. Where neurite outgrowth extended beyond a single field two overlapping images were combined. Two measurements of radial outgrowth were recorded for each ganglion (maximal outgrowth from ganglia to the ends of the most distal neurites) on each day to give a ganglion average.

Vincristine sulphate (Sigma), dissolved in DMSO, was added to SCG cultures every day in fresh media at a final concentration of 1 nM from DIV5 onwards. Phase contrast images of the same field of neurites were captured (20x objective) at 0, 3 and 6 days after vincristine addition. The Degeneration Index of distal neurites was calculated using ImageJ essentially as described previously (30), except that a size range of 10-350 pixels was used for calculating the area constituting degenerated axon fragments in the 1376 x 1032 pixel images.

Neurite transection assays were performed in the same SCG cultures used for the assessment of neurite outgrowth. Neurites were cut at DIV8 with a scalpel at a point roughly midway between the ganglion and their distal ends. Phase contrast images of the same field of cut neurites were captured (20x objective) at 1-2 h intervals after cut as indicated. The Degeneration Index of cut neurites was calculated as above except that the range of pixels used for calculating the area constituting degenerated axon fragments was adjusted to account for differing neurite densities between dishes. A size range of 10-350 pixels was used for fields with dense neurites and 10-200 pixels was used for fields with sparse neurites (in 1376 x 1032 pixel images captured using the 20x objective) with the same settings being applied to the same field of neurites at all timepoints.

Statistical analyses.

The numbers of samples and/or the age, sex and numbers of mice used in each individual experiment are described in the relevant section of the main text or figure legend. Statistical testing of data was performed using Prism (GraphPad Software Inc., La Jolla, USA). The appropriate tests used are described in the Figure legends. A p value < 0.05 was considered significant.

ACKNOWLEDGEMENTS

This work was funded by an Institute Strategic Programme Grant from the UK Biotechnology and Biological Sciences Research Council, UK Medical Research Council Grant MR/N004582/1 and The Ruth K. Broad Biomedical Research Foundation.

CONFLICT OF INTEREST STATEMENT

The authors declare no competing financial interests.

AUTHOR CONTRIBUTIONS

JG and MPC conceived the study. JG designed and performed all experiments. JG and MPC and co-wrote the manuscript with input from GY and PM who generated mice with the *Nmnat2*^{gtBay} gene trap allele.

REFERENCES

1 Conforti, L., Gilley, J. and Coleman, M.P. (2014) Wallerian degeneration: an emerging axon death pathway linking injury and disease. *Nat. Rev. Neurosci.*, **15**, 394-409.

2 Conforti, L., Janeckova, L., Wagner, D., Mazzola, F., Cialabrini, L., Di Stefano, M., Orsomando, G., Magni, G., Bendotti, C., Smyth, N. *et al.* (2011) Reducing expression of NAD+ synthesizing enzyme NMNAT1 does not affect the rate of Wallerian degeneration. *FEBS J.*, **278**, 2666-2679.

3 Gilley, J., Adalbert, R., Yu, G. and Coleman, M.P. (2013) Rescue of Peripheral and CNS Axon Defects in Mice Lacking NMNAT2. *J. Neurosci.*, **33**, 13410-13424.

4 Gilley, J. and Coleman, M.P. (2010) Endogenous Nmnat2 is an essential survival factor for maintenance of healthy axons. *PLoS Biol.*, **8**, e1000300.

5 Hicks, A.N., Lorenzetti, D., Gilley, J., Lu, B., Andersson, K.E., Miligan, C., Overbeek, P.A., Oppenheim, R. and Bishop, C.E. (2012) Nicotinamide mononucleotide adenylyltransferase 2 (Nmnat2) regulates axon integrity in the mouse embryo. *PLoS One*, **7**, e47869.

6 Hikosaka, K., Ikutani, M., Shito, M., Kazuma, K., Gulshan, M., Nagai, Y., Takatsu, K., Konno, K., Tobe, K., Kanno, H. *et al.* (2014) Deficiency of nicotinamide mononucleotide adenylyltransferase 3 (Nmnat3) causes hemolytic anemia by altering the glycolytic flow in mature erythrocytes. *J. Biol. Chem.*, **289**, 14796-14811.

7 Di Stefano, M., Loreto, A., Orsomando, G., Mori, V., Zamporlini, F., Hulse, R.P., Webster, J., Donaldson, L.F., Gering, M., Raffaelli, N. *et al.* (2017) NMN Deamidase Delays

Wallerian Degeneration and Rescues Axonal Defects Caused by NMNAT2 Deficiency In Vivo. *Curr. Biol.*, **27**, 784-794.

8 Gilley, J., Orsomando, G., Nascimento-Ferreira, I. and Coleman, M.P. (2015) Absence of SARM1 Rescues Development and Survival of NMNAT2-Deficient Axons. *Cell Rep.*, **10**, 1974-1981.

9 Gilley, J., Ribchester, R.R. and Coleman, M.P. (2017) Sarm1 Deletion, but Not Wld(S), Confers Lifelong Rescue in a Mouse Model of Severe Axonopathy. *Cell Rep.*, **21**, 10-16.

10 Davies, G., Lam, M., Harris, S.E., Trampush, J.W., Luciano, M., Hill, W.D., Hagenaars, S.P., Ritchie, S.J., Marioni, R.E., Fawns-Ritchie, C. *et al.* (2018) Study of 300,486 individuals identifies 148 independent genetic loci influencing general cognitive function. *Nat. Commun.*, **9**, 2098.

11 Ali, Y.O., Allen, H.M., Yu, L., Li-Kroeger, D., Bakhshizadehmahmoudi, D., Hatcher, A., McCabe, C., Xu, J., Bjorklund, N., Taglialatela, G. *et al.* (2016) NMNAT2:HSP90 Complex Mediates Proteostasis in Proteinopathies. *PLoS Biol.*, **14**, e1002472.

12 Ali, Y.O., Li-Kroeger, D., Bellen, H.J., Zhai, R.G. and Lu, H.C. (2013) NMNATs, evolutionarily conserved neuronal maintenance factors. *Trends Neurosci.*, **36**, 632-640.

13 Ljungberg, M.C., Ali, Y.O., Zhu, J., Wu, C.S., Oka, K., Zhai, R.G. and Lu, H.C. (2012) CREB-activity and nmnat2 transcription are down-regulated prior to neurodegeneration, while NMNAT2 over-expression is neuroprotective, in a mouse model of human tauopathy. *Hum. Mol. Genet.*, **21**, 251-267.

14 Slivicki, R.A., Ali, Y.O., Lu, H.C. and Hohmann, A.G. (2016) Impact of Genetic Reduction of NMNAT2 on Chemotherapy-Induced Losses in Cell Viability In Vitro and Peripheral Neuropathy In Vivo. *PLoS One*, **11**, e0147620.

15 Mayer, P.R., Huang, N., Dewey, C.M., Dries, D.R., Zhang, H. and Yu, G. (2010) Expression, localization, and biochemical characterization of nicotinamide mononucleotide adenylyltransferase 2. *J. Biol. Chem.*, **285**, 40387-40396.

16 Rigaud, M., Gemes, G., Barabas, M.E., Chernoff, D.I., Abram, S.E., Stucky, C.L. and Hogan, Q.H. (2008) Species and strain differences in rodent sciatic nerve anatomy: implications for studies of neuropathic pain. *Pain*, **136**, 188-201.

17 Conforti, L., Wilbrey, A., Morreale, G., Janeckova, L., Beirowski, B., Adalbert, R., Mazzola, F., Di Stefano, M., Hartley, R., Babetto, E. *et al.* (2009) Wld S protein requires Nmnat activity and a short N-terminal sequence to protect axons in mice. *J. Cell Biol.*, **184**, 491-500.

18 Gerdts, J., Summers, D.W., Sasaki, Y., Diantonio, A. and Milbrandt, J. (2013) Sarm1-Mediated Axon Degeneration Requires Both SAM and TIR Interactions. *J. Neurosci.*, **33**, 13569-13580.

19 Wang, M., Wu, Y., Culver, D.G. and Glass, J.D. (2001) The gene for slow Wallerian degeneration (Wld(s)) is also protective against vincristine neuropathy. *Neurobiol. Dis.*, **8**, 155-161.

20 LaPointe, N.E., Morfini, G., Brady, S.T., Feinstein, S.C., Wilson, L. and Jordan, M.A. (2013) Effects of eribulin, vincristine, paclitaxel and ixabepilone on fast axonal transport and kinesin-1 driven microtubule gliding: implications for chemotherapy-induced peripheral neuropathy. *Neurotoxicology*, **37**, 231-239.

21 Lek, M., Karczewski, K.J., Minikel, E.V., Samocha, K.E., Banks, E., Fennell, T., O'Donnell-Luria, A.H., Ware, J.S., Hill, A.J., Cummings, B.B. *et al.* (2016) Analysis of protein-coding genetic variation in 60,706 humans. *Nature*, **536**, 285-291.

22 Bartha, I., di Iulio, J., Venter, J.C. and Telenti, A. (2018) Human gene essentiality. *Nat. Rev. Genet.*, **19**, 51-62.

23 Geisler, S., Doan, R.A., Strickland, A., Huang, X., Milbrandt, J. and DiAntonio, A. (2016) Prevention of vincristine-induced peripheral neuropathy by genetic deletion of SARM1 in mice. *Brain*, **139**, 3092-3108.

24 Milde, S., Adalbert, R., Elaman, M.H. and Coleman, M.P. (2015) Axonal transport declines with age in two distinct phases separated by a period of relative stability. *Neurobiol. Aging*, **36**, 971-981.

25 Milde, S., Gilley, J. and Coleman, M.P. (2013) Subcellular localization determines the stability and axon protective capacity of axon survival factor nmnat2. *PLoS Biol.*, **11**, e1001539.

26 Dubin, A.E. and Patapoutian, A. (2010) Nociceptors: the sensors of the pain pathway. *J. Clin. Invest.*, **120**, 3760-3772.

27 Vriens, J., Nilius, B. and Voets, T. (2014) Peripheral thermosensation in mammals. *Nat. Rev. Neurosci.*, **15**, 573-589.

28 Cain, D.M., Khasabov, S.G. and Simone, D.A. (2001) Response properties of mechanoreceptors and nociceptors in mouse glabrous skin: an in vivo study. *J. Neurophysiol.*, **85**, 1561-1574.

29 Koltzenburg, M., Stucky, C.L. and Lewin, G.R. (1997) Receptive properties of mouse sensory neurons innervating hairy skin. *J. Neurophysiol.*, **78**, 1841-1850.

30 Sasaki, Y., Vohra, B.P., Lund, F.E. and Milbrandt, J. (2009) Nicotinamide mononucleotide adenylyl transferase-mediated axonal protection requires enzymatic activity but not increased levels of neuronal nicotinamide adenine dinucleotide. *J. Neurosci.*, **29**, 5525-5535.

LEGENDS TO FIGURES

Figure 1. Mice with graded levels of *Nmnat2* expression are viable and overtly normal.

(A) Genotype frequencies of viable offspring from crosses between *Nmnat2*$^{+/gtE}$ and *Nmnat2*$^{+/gtBay}$ mice. The observed birth frequencies are not significantly different from expected frequencies: $\chi^2 = 0.583$, d.f. = 3, p = 0.9004. (B) Body weights of male and female mice of the indicated genotypes at 5-8 months and female mice at 21-24 months. Individual mouse weights with means ±SEM are plotted. n.s. = not significant [p > 0.05], separate one-way ANOVA for males and females at each age with Dunnett's multiple comparison tests (relative to wild-types). (C) Quantification of endpoint RT-PCR analysis of relative *Nmnat2* mRNA levels in the brains of 6 month wild-type, *Nmnat2*$^{+/gtBay}$, *Nmnat2*$^{+/gtE}$ and *Nmnat2*$^{gtBay/gtE}$ mice. Data are presented as the mean percentage ± SEM of wild-type levels after normalization to *Actb* mRNA levels. * p < 0.05, ** p <0.01 and *** p < 0.001, one-way ANOVA with Tukey's multiple comparison tests (n = 4 sets of each genotype).

Figure 2. Early deficiency and later loss of myelinated tibial nerve axons in *Nmnat2* compound heterozygote mice.

(A) Numbers of myelinated axons in tibial nerves of mice of the indicated genotypes and ages (n = 4-5 per genotype at each age). Individual values and means ±SEM are plotted. n.s. = not significant [p > 0.05] and *** p < 0.001, separate one-way ANOVA for each age with Tukey's multiple comparison tests. (B) Numbers of myelinated axons in tibial nerves of mice of the indicated genotypes and ages (n = 4-5 per genotype at each age). Individual values and means ±SEM are plotted. n.s. = not significant [p > 0.05] and *** p < 0.001, two-way ANOVA with Bonferroni's multiple comparison tests for effects within genotypes (selected results shown). (C) Complete tibial nerve cross-sections stained with FluoroMyelin™ Red from mice of the

indicated genotypes and ages (representative of n = 4-5 per genotype). (D) Plots of axon counts, nerve cross-sectional area and axon density for tibial nerves from *Nmnat2*$^{gtBay/gtE}$ compound heterozygote mice at the indicated ages as a percentage of that in wild-type tibial nerves (n = 4-5 nerves per genotype at each age).

Figure 3. Early deficiency of myelinated axons in L3 dorsal root and later changes to myelinated axons in L3 ventral root in *Nmnat2* compound heterozygote mice.

(A) Numbers of myelinated axons in L3 dorsal roots of mice of the indicated genotypes and ages (n = 4-5 per genotype at each age). Individual values and means ±SEM are plotted. n.s. = not significant [$p > 0.05$] and *** $p < 0.001$, two-way ANOVA with Bonferroni's multiple comparison tests. (B) Distribution of axon diameters in 6 month old wild-type and *Nmnat2*$^{gtBay/gtE}$ compound heterozygote L3 dorsal roots. Mean distribution ±SEM is plotted for total numbers of axons in three roots of each genotype calculated from a random sample of at least 145 axons per root. n.s. = not significant [$p > 0.05$] and *** $p < 0.001$, two-way ANOVA with Sidak's multiple comparisons for between genotype effects. (C) Cross-sections of L3 dorsal root myelinated axons stained with FluoroMyelin™ Red from 24 month old mice of the indicated genotypes (representative of n = 5 per genotype). (D) Numbers of myelinated axons in L3 ventral roots of mice of the indicated genotypes and ages (n = 4-5 per genotype at each age). Individual values and means ±SEM are plotted. n.s. = not significant [$p > 0.05$] and * $p < 0.05$, two-way ANOVA with Bonferroni's multiple comparison tests. (E) Cross-sections of L3 ventral root myelinated axons stained with FluoroMyelin™ Red from mice of the indicated genotypes and ages (representative of n = 4-5 per genotype). Axons with thin myelin sheaths, resembling regenerating axons, are labelled with asterisks. (F) Number of myelinated axons in L3 ventral roots of 24 month old mice of the indicated genotypes (n = 5 per genotype) grouped based on the status of their myelin sheaths. Axons with normal thickness myelin were classed

as “healthy”, those with invaginations, evaginations or wide incisures as “abnormal” and those with thin myelin (relative to axon diameter) as “thin”. Individual values and means ±SEM are plotted. n.s. = not significant [$p > 0.05$], * $p < 0.05$ and ** $p < 0.01$, individual *t* tests for each class of axons.

Figure 4. Touch sensitivity is normal in *Nmnat2*$^{gtBay/gtE}$ compound heterozygote but thermal perception and Rotarod performance are both altered.

(A) Force at paw withdrawal (left graph) and latency to paw withdrawal (right graph) for 6-9 month old male mice of the indicated genotypes (n = 9-12 per genotype) in the dynamic plantar aesthesiomter test. Individual values and means ±SEM are plotted. n.s. = not significant [$p > 0.05$], one-way ANOVA with Tukey’s multiple comparison tests. (B) Percentage time spent at the test temperature for 6-9 month old male mice of the indicated genotypes (n = 9-12 per genotype) in the two-place temperature preference test (control plate at 30°C). Means ±SEM are plotted. n.s. = not significant [$p > 0.05$], separate one-way ANOVA for each test temperature with Tukey’s multiple comparison tests. (C and D) Latency to fall for female mice of the indicated genotypes in a longitudinal Rotarod analysis between the ages of 6 and 24 months. Means ±SEM for the same data are plotted in alternative ways to highlight different statistical differences: n.s. = not significant [$p > 0.05$], ** $p < 0.01$ and *** $p < 0.001$, two-way ANOVA with Dunnett’s multiple comparison tests for age effects (relative to 6 months) within each genotype in (C); n.s. = not significant [$p > 0.05$] and ** $p < 0.01$, two-way ANOVA with Tukey’s multiple comparison tests for effects between genotypes at each age in (D). (E) Body weights of mice at each test age in the Rotarod analysis described in (C and D). Means ±SEM are plotted. There is no statistically-significant difference in body weight between genotypes at any age (two-way ANOVA with Tukey’s multiple comparison tests).

Figure 5. Altered outgrowth and survival of *Nmnat2*$^{gtBay/gtE}$ compound heterozygote SCG neurites.

(A) Representative images of neurite outgrowth at DIV5 in SCG explant cultures of the indicated genotypes. (B) Quantification of neurite outgrowth in SCG explant cultures of the indicated genotypes between DIV0 and DIV7. Mean outgrowth ±SEM is plotted for ganglia from n = 3-4 embryos per genotype. n.s. = not significant [$p > 0.05$], ** $p < 0.01$ and *** $p < 0.001$, two-way ANOVA with Tukey's multiple comparisons for between genotype effects at each timepoint. (C) Representative images of neurites in SCG explant cultures of the indicated genotypes after 144 h of daily 1 nM vincristine treatment or without treatment. (D) Quantification of the degeneration index (DI) of neurites in SCG explant cultures of the indicated genotypes at various times after starting daily 1 nM vincristine treatment or without treatment. Mean DI ±SEM is plotted for ganglia from n = 3 embryos per genotype. n.s. = not significant [$p > 0.05$], ** $p < 0.01$ and *** $p < 0.001$, two-way ANOVA with Tukey's multiple comparisons for between genotype effects at each timepoint. (E) Representative images of transected SCG neurites of the indicated genotypes at the time of cut (0h cut) and 4 h after cut (4h cut). (F) Quantification of the degeneration index (DI) of transected SCG neurites of the indicated genotypes at various times after cut. Mean DI ±SEM (left graph) and mean change in DI (right graph) are plotted for ganglia from n = 3-4 embryos per genotype. n.s. = not significant [$p > 0.05$], * $p < 0.05$, ** $p < 0.01$ and *** $p < 0.001$, two-way ANOVA with Tukey's multiple comparisons for between genotype effects at each timepoint.

ABBREVIATIONS

NMNAT; nicotinamide mononucleotide adenylyltransferase

Wld^{S} ; slow Wallerian degeneration

SARM1; sterile alpha and TIR motif-containing protein 1

NAD; nicotinamide adenine dinucleotide

NMN; nicotinamide mononucleotide

PNS; peripheral nervous system

CNS; central nervous system

SNP; single nucleotide polymorphism

DRG; dorsal root ganglion

SCG; superior cervical ganglion

DIV; days *in vitro*

A

cross	viable offspring		
	Genotype	**Observed**	*Expected*
Nmnat2$^{+/gtBay}$ x *Nmnat2*$^{+/gtE}$	*wild-type*	**241**	*238.5*
	Nmnat2$^{+/gtBay}$	**245**	*238.5*
	Nmnat2$^{+/gtE}$	**239**	*238.5*
	Nmnat2$^{gtBay/gtE}$	**229**	*238.5*

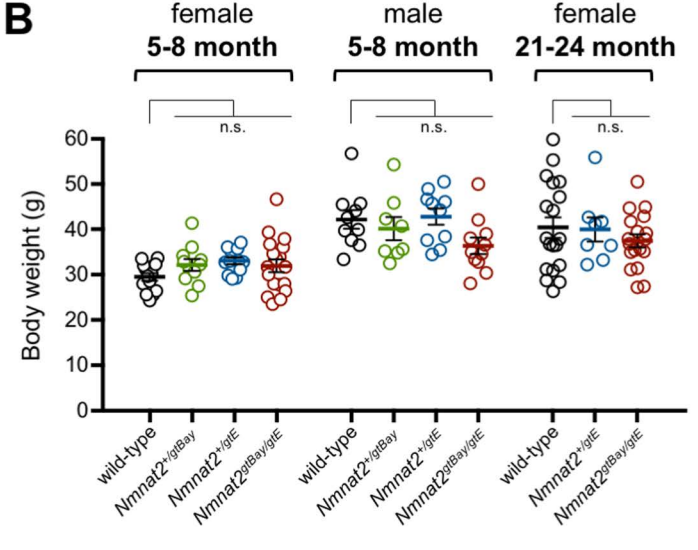

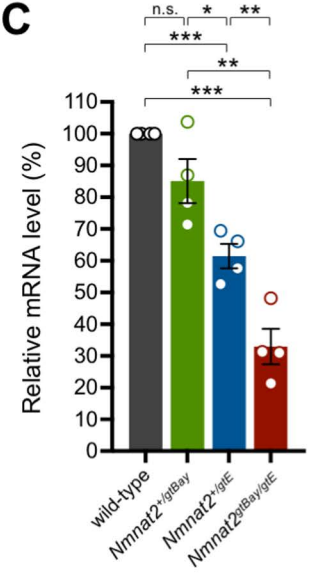

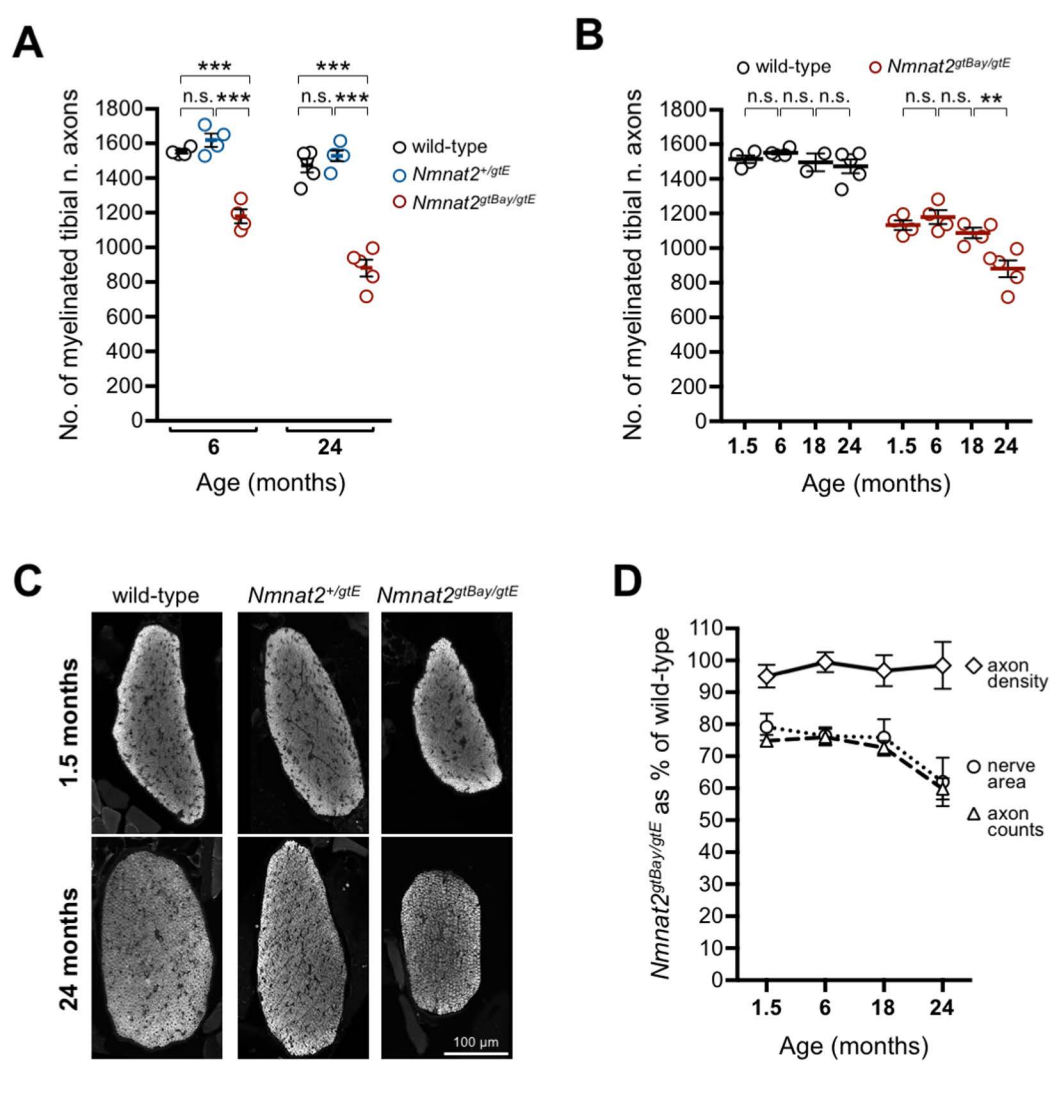
A
***
n.s.
***
***
n.s.
***
wild-type
Nmnat2+/gtE
Nmnat2gtBay/gtE
No. of myelinated tibial n. axons
1800
1600
1400
1200
1000
800
600
400
200
0
6
24
Age (months)
B
wild-type
Nmnat2gtBay/gtE
n.s.
n.s.
n.s.
n.s.
n.s.
**
No. of myelinated tibial n. axons
1.5
6
18
24
1.5
6
18
24
Age (months)
C
wild-type
Nmnat2+/gtE
Nmnat2gtBay/gtE
1.5 months
24 months
100 µm
D
Nmnat2gtBay/gtE as % of wild-type
110
100
90
80
70
60
50
40
30
20
10
0
axon density
nerve area
axon counts
1.5
6
18
24
Age (months)

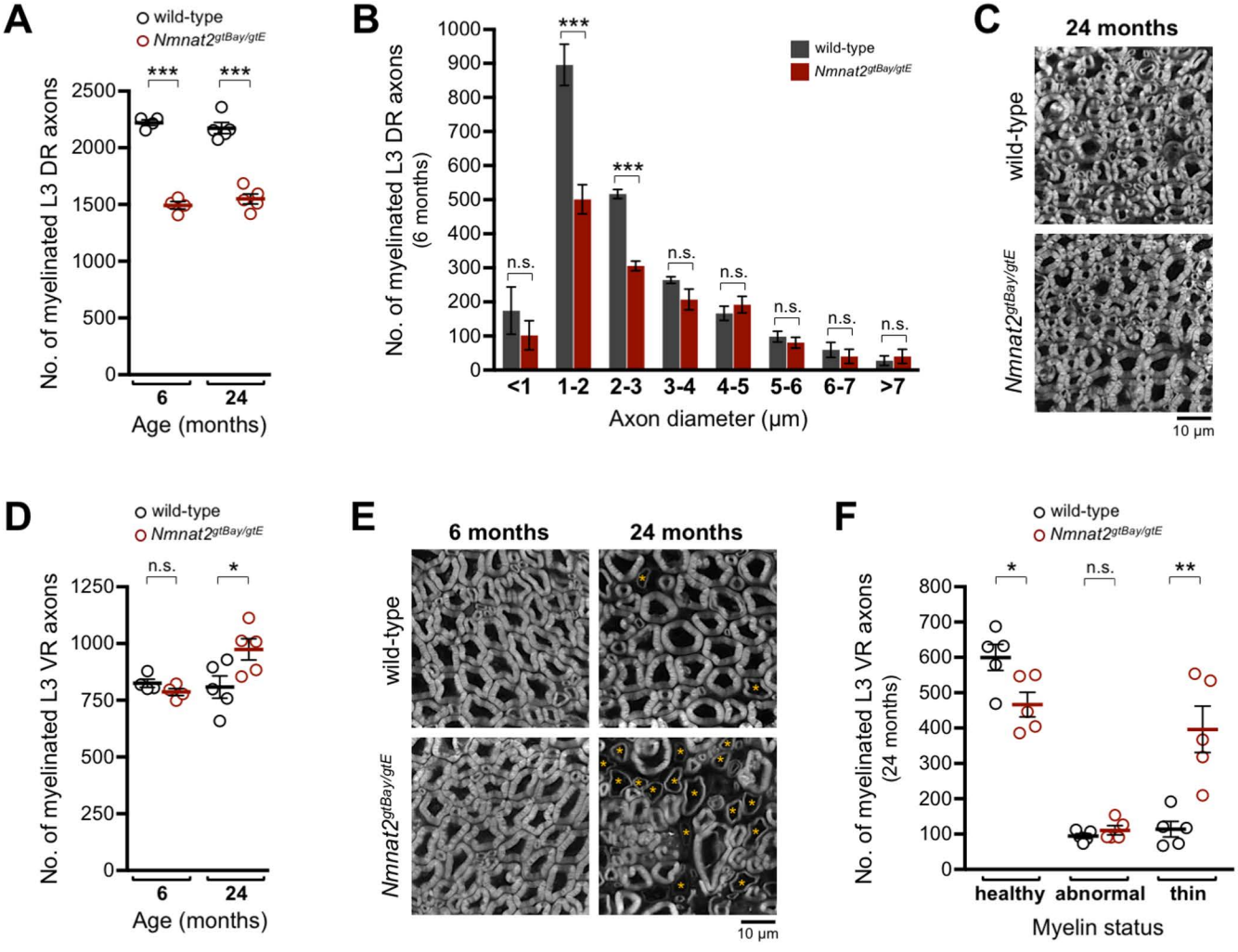
A
wild-type
Nmnat2gtBay/gtE
No. of myelinated L3 DR axons
***
***
2500
2000
1500
1000
500
0
6
24
Age (months)
B
No. of myelinated L3 DR axons
(6 months)
wild-type
Nmnat2gtBay/gtE
1000
900
800
700
600
500
400
300
200
100
0
***
***
n.s.
n.s.
n.s.
n.s.
n.s.
<1
1-2
2-3
3-4
4-5
5-6
6-7
>7
Axon diameter (μm)
C
24 months
wild-type
Nmnat2gtBay/gtE
10 μm
D
wild-type
Nmnat2gtBay/gtE
No. of myelinated L3 VR axons
n.s.
*
1250
1000
750
500
250
0
6
24
Age (months)
E
6 months
24 months
wild-type
Nmnat2gtBay/gtE
10 μm
F
wild-type
Nmnat2gtBay/gtE
No. of myelinated L3 VR axons
(24 months)
*
n.s.
**
800
700
600
500
400
300
200
100
0
healthy
abnormal
thin
Myelin status

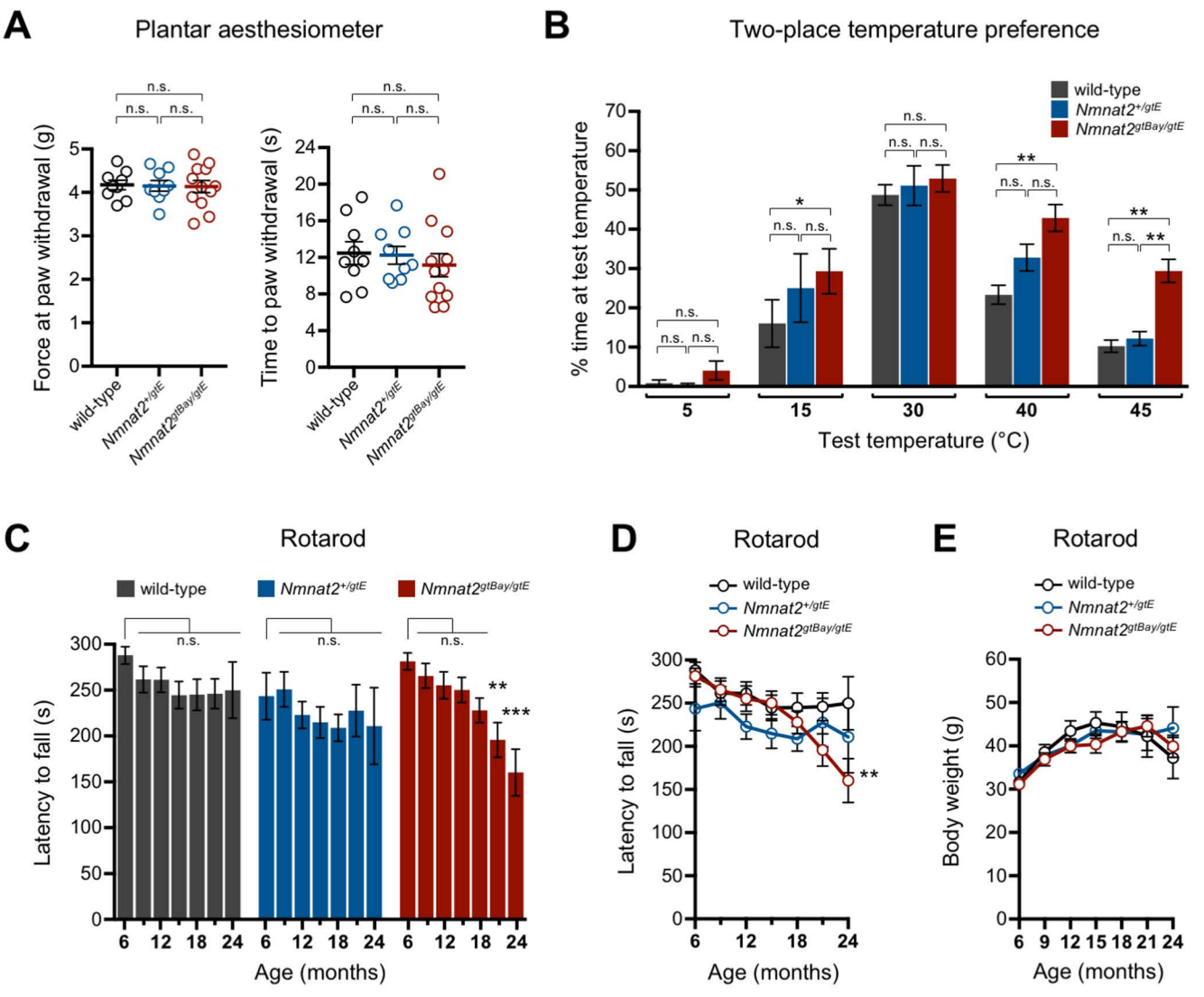
A
Plantar aesthesiometer
Force at paw withdrawal (g)
Time to paw withdrawal (s)
n.s.
wild-type
Nmnat2+/gtE
Nmnat2gtBay/gtE
B
Two-place temperature preference
% time at test temperature
Test temperature (°C)
5
15
30
40
45
*
**
C
Rotarod
Latency to fall (s)
Age (months)
***
D
Rotarod
E
Rotarod
Body weight (g)

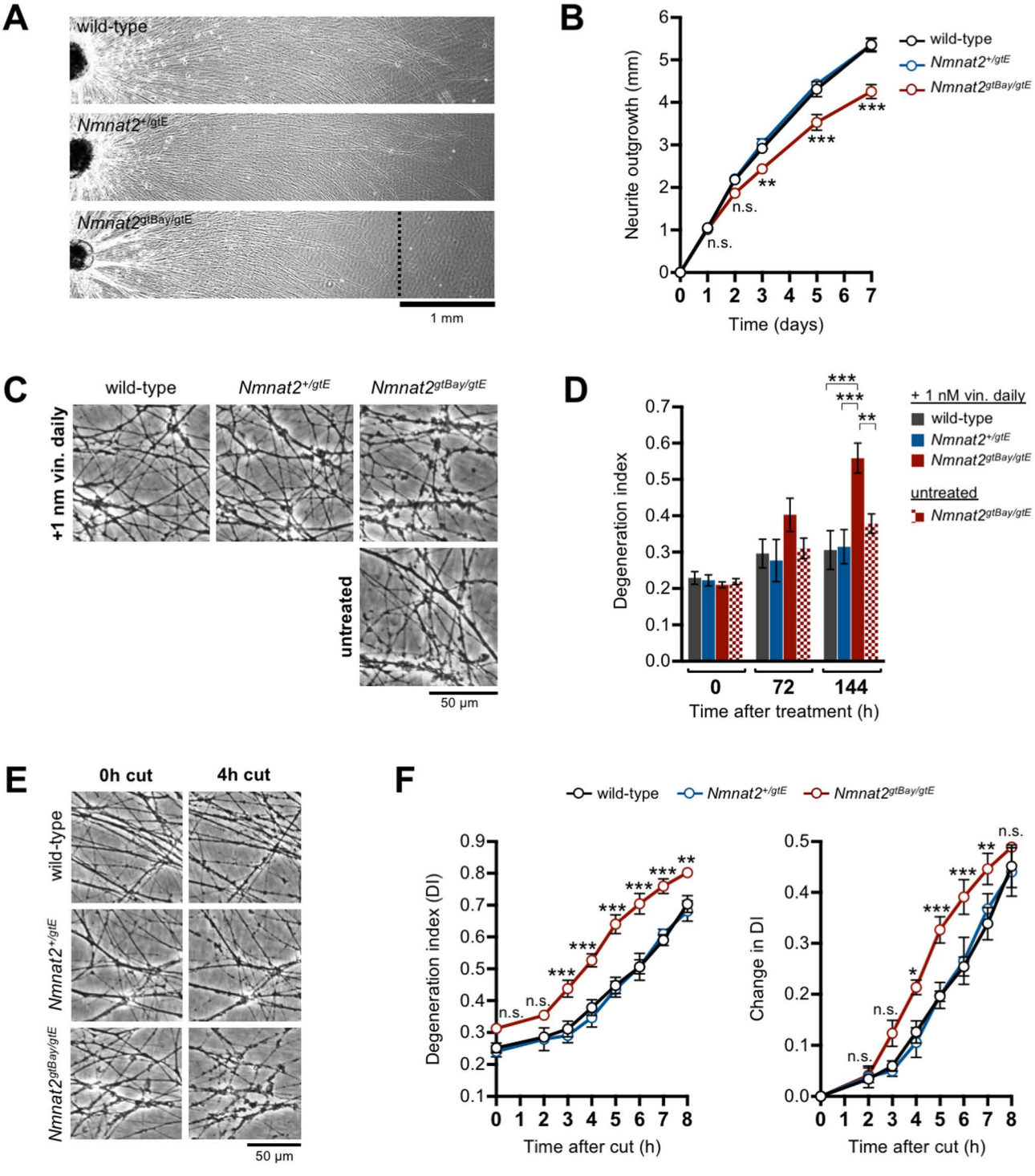
A
wild-type
Nmnat2+/gtE
Nmnat2gtBay/gtE
1 mm
B
Neurite outgrowth (mm)
Time (days)
wild-type
Nmnat2+/gtE
Nmnat2gtBay/gtE
n.s.
n.s.
**
***
***
C
wild-type
Nmnat2+/gtE
Nmnat2gtBay/gtE
+1 nm vin. daily
untreated
50 µm
D
Degeneration index
Time after treatment (h)
+ 1 nM vin. daily
wild-type
Nmnat2+/gtE
Nmnat2gtBay/gtE
untreated
Nmnat2gtBay/gtE
E
0h cut
4h cut
wild-type
Nmnat2+/gtE
Nmnat2gtBay/gtE
50 µm
F
wild-type
Nmnat2+/gtE
Nmnat2gtBay/gtE
Degeneration index (DI)
Time after cut (h)
Change in DI
Time after cut (h)